

## Article

# The Characterization of a Biodegradable Mg Alloy after Powder Bed Fusion with Laser Beam/Metal Processing for Custom Shaped Implants

Doina Raducanu <sup>1</sup>, Vasile Danut Cojocaru <sup>1</sup> , Anna Nocivin <sup>2,\*</sup> , Silviu Iulian Drob <sup>3</sup>, Radu Emil Hendea <sup>4</sup>, Doina Stanciu <sup>5</sup> , Steliana Ivanescu <sup>5</sup> , Vlad Andrei Raducanu <sup>6</sup>, Nicolae Serban <sup>1</sup> , Elisabeta Mirela Cojocaru <sup>1</sup> and Radu Septimiu Campian <sup>4</sup>

<sup>1</sup> Department of Metallic Materials Processing and Ecometallurgy, University POLITEHNICA of Bucharest, 060042 Bucharest, Romania; doina.raducanu@upb.ro (D.R.); dan.cojocaru@upb.ro (V.D.C.); nicolae.serban@upb.ro (N.S.); elisabeta.cojocaru@upb.ro (E.M.C.)

<sup>2</sup> Faculty of Mechanical, Industrial and Maritime Engineering, OVIDIUS University of Constanta, 900527 Constanta, Romania

<sup>3</sup> Institute of Physical Chemistry "Ilie Murgulescu", Romanian Academy, Spl. Independentei 202, 060021 Bucharest, Romania; sidrob.icf@gmail.com

<sup>4</sup> Department of Oral Rehabilitation, Faculty of Dental Medicine, Iuliu Hatieganu University of Medicine and Pharmacy, 400349 Cluj-Napoca, Romania; raduhendea@yahoo.com (R.E.H.); rcampian@email.com (R.S.C.)

<sup>5</sup> ZIRCON DENT SRL, 400690 Cluj-Napoca, Romania; doinastanciu09@yahoo.com (D.S.); sivanescu@yahoo.com (S.I.)

<sup>6</sup> Faculty of Decorative Arts and Design, National University of Arts, 010702 Bucharest, Romania; andrei.raducanu@unarte.org

\* Correspondence: anocivin@univ-ovidius.ro



**Citation:** Raducanu, D.; Cojocaru, V.D.; Nocivin, A.; Drob, S.I.; Hendea, R.E.; Stanciu, D.; Ivanescu, S.; Raducanu, V.A.; Serban, N.; Cojocaru, E.M.; et al. The Characterization of a Biodegradable Mg Alloy after Powder Bed Fusion with Laser Beam/Metal Processing for Custom Shaped Implants. *Materials* **2024**, *17*, 1682. <https://doi.org/10.3390/ma17071682>

Academic Editor: Jaroslaw Jakubowicz

Received: 12 March 2024

Revised: 1 April 2024

Accepted: 3 April 2024

Published: 6 April 2024



**Copyright:** © 2024 by the authors. Licensee MDPI, Basel, Switzerland. This article is an open access article distributed under the terms and conditions of the Creative Commons Attribution (CC BY) license (<https://creativecommons.org/licenses/by/4.0/>).

**Abstract:** A new Mg-Zn-Zr-Ca alloy in a powder state, intended to be used for custom shaped implants, was obtained via a mechanical alloying method from pure elemental powder. Further, the obtained powder alloy was processed by a PBF-LB/M (powder bed fusion with laser beam/of metal) procedure to obtain additive manufactured samples for small biodegradable implants. A series of microstructural, mechanical and corrosion analyses were performed. The SEM (scanning electron microscopy) analysis of the powder alloy revealed a good dimensional homogeneity, with a uniform colour, no agglutination and almost rounded particles, suitable for the powder bed fusion procedure. Further, the PBF-LB/M samples revealed a robust and unbreakable morphology, with a suitable porosity (that can reproduce that of cortical bone) and without an undesirable balling effect. The tested Young's modulus of the PBF-LB/M samples, which was 42 GPa, is close to that of cortical bone, 30 GPa. The corrosion tests that were performed in PBS (Phosphate-buffered saline) solution, with three different pH values, show that the corrosion parameters have a satisfactory evolution comparative to the commercial ZK 60 alloy.

**Keywords:** Mg alloys; mechanical alloying; laser powder bed fusion for metals; mechanical testing; corrosion resistance

## 1. Introduction

Apart from well-known fields of use, such as the automotive field, aerospace and electronics, magnesium alloys are currently widely tested as biomedical components, not only for their high strength-to-weight ratio [1,2], but also for their good structural and mechanical biocompatibility [3,4]. Moreover, in a series of biocompatible materials, magnesium alloys fall under the category of biodegradable materials [5,6], a very useful physical process that prevents a second surgery for removing an anterior inserted bone implant after bone healing due to the fact that magnesium can easily disintegrate in time in human physiological environments [7]. Therefore, if used as temporary orthopaedic implant, novel Mg

alloys can replace other bone implants, like Ti-alloys, achieving mechanical performances of human bone by avoiding unwanted stress-shielding effects [8–10] and promoting bone remodelling and healing [11–13].

The main advantages of using magnesium alloy for bone implants refers to the fact that it exhibits mechanical performances similar to human bone (a low density of  $1.74 \text{ g/cm}^3$  and a low elastic modulus of about 40–44 GPa, very close to that of cortical bone at 30 GPa, [14]) and, during degradation in human environments, it represents an essential nutrient which promotes bone growth and mineralization [8]. The main disadvantage is the risk of more the rapid degradation of magnesium alloy prior to the bone healing process, a fact that requires a difficult co-ordination between the two processes: degradation versus healing [15,16]. Fortunately, the corrosion products that result from the degradation process are non-toxic and can be easily eliminated through the body's metabolism [15]. However,  $\text{H}_2$  gas, as a corrosion product, can be accumulated in the surrounding tissue as gas bubbles, causing the separation of tissue layers [17,18], and  $\text{OH}^-$  ions, as another possible corrosion product, can produce surface alkalization and likely the degradation of cells [19]. But *in vivo* tests showed that the circulation of body fluids facilitates the evacuation of corrosion products that are more abundant in the tissue surrounding the implant in the first period after implantation, and, consequently, the local inflammation is reduced within a matter of days [20,21].

Nowadays, numerous efforts are made to improve the mechanical and biological performances of Mg alloys. One way of action in this direction is the metallurgical optimizing of the chemical composition of the alloy with suitable alloying elements, which allow for obtaining microstructures that are much more adapted to biocompatibility requirements. Another method of action refers to the technological modalities of designing and obtaining a proper bone implant, or even a personalized one.

Referring to the chemical composition, Mg-Zn-Zr alloys (ZK) seem to have superior biocompatibility than already tested Mg-Al-Zn (AZ) or Mg-Zn-RE (WE) [22,23]. Unfortunately, it has been reported that aluminium ions denote a high score for inducing neurotoxicity and brain disorders (Alzheimer's), and, on the other hand, rare elements, such as Ce, Y and Pr, can induce severe hepatotoxicity even if they can reduce the corrosion rate of these alloys [23]. But for ZK alloys, zinc and zirconium, alongside other possible alloying elements such as Ca, Mn, Si or Ag, arouse real interest in the research world due to their high biosafety [24,25]. Thus, zinc, as one possible alloying element for ZK alloys, has an antimicrobial effect against bacteria in the implantation area [26], being at the same time an important micronutrient for supporting the immune system and enzymatic reactions [27,28]. On the other hand, zinc is reported to improve the mechanical properties of magnesium alloys, decreasing their degradation rate and increasing the osteoblastic cells proliferation during bone reconstruction [28]. When the degradation phenomenon of magnesium alloy occurs, the resulting zinc can be eliminated through the gastrointestinal tract, urine or skin [29,30]. Biological studies have shown that a zinc content of up to 14.5 (%wt.) is beneficial for the human body, above which an unwanted cytotoxicity of the alloy appears [31]. Zirconium, as another important alloying element, is also a biocompatible one, with low ionic toxicity, improving at the same time the corrosion resistance and mechanical properties of the magnesium alloys, even in small amounts [32]. At the same time, zirconium is bioinert if it collects in small amounts in bone or the nervous systems [32]. Calcium, in turn, as a main mineral of bone components [33], represents another potential and important alloying element to magnesium alloys, with a low density ( $1.55 \text{ g/cm}^3$ ) also; research works, such as [34,35], report the exceptional biocompatibility of the binary Mg-Ca alloys. It should also be emphasized that calcium facilitates the hydroxyapatite generation, thereby helping with bone healing [36,37]. Regarding the corrosion resistance of magnesium alloys, calcium, through a controlled composition, can also decrease the corrosion rate, reducing the grain size in the obtained structure [38,39].

Therefore, it would be believed that a promising alternative to the experimental tests carried out so far on ZK ternary alloys (Mg-Zn-Zr) and binary Mg-Ca alloys would be

those that include all three alloying elements: Zn, Zr and Ca. Thus, the variant selected for study in the present work has alloying elements with compositions that largely converge with those studied so far, being a new one anyway, and only being reported by the present group of authors. All three alloying elements have a limited solubility in magnesium: zinc, until 6.2%wt. at 340 °C [40]; zirconium, until 0.87%wt. at 700 °C [41]; and calcium, until 1.11%wt. at 521 °C [33]. However, in conformity with [7], if the procedure of the alloy obtaining can induce an extent of these solubilities and reach a non-equilibrium supersaturated solid solution, without secondary phases, the corrosion resistance of the alloy can be evidently improved. Therefore, for the present study, a similar/close situation/case was considered when selecting the not-studied-before chemical composition Mg-10Zn-0.8Ca-0.5Zr (%wt.). As a consequence, apart from chemical composition designing, new technological modalities of obtaining and processing these alloys in a final fabricated bone implant are planned nowadays, even in a personalised design [42,43]. Standard designs of implants are destined for large groups of patients. However, to help with the surgeon's work of ensuring a precise fit for each particular case of patients' bones, in recent years, what is developing more and more is the trend of the personalization of implants using modern additive manufacturing (AM) procedures. For the next five years, the production of personalized (AM) implants is estimated to reach about USD 70 billion [29].

The alloy selected for study (Mg-10Zn-0.8Ca-0.5Zr (%wt.)) has been proposed and used in a modern AM method, named PBF-LB/M (powder bed fusion-with laser beam/of metal), a method that can assure improved biocompatible and biodegradable implants with custom shaped designs, and with controlled porosities necessary to easily initiate bone regeneration.

The PBF-LB/M method of additive manufacturing represents a powder bed fusion process which uses a high-density laser beam (L-PBF) on a micro scale [44–46]. This method can assure a rapid manufacture of the implants' metallic parts with custom geometries, without the need for post-processing [31,47]. Therefore, maximum attention should be afforded to the pre-processing step of PBF-LB/M, i.e., the CAD (computer-aided design) of the printed model. The final quality of the obtained product is dictated by the selected process parameters, such as the laser power, scanning speed, distance between the printed layers and distance from the hatch. The PBF-LB/M method can be considered one of the most efficient variants of AM due to its high dimensional accuracy between as-built geometry and the designed geometry, even if some inadvertences can occur like possible balling effects or some misoriented growth in microstructure. In the case of magnesium and its alloys, which are reactive metallic materials, an inert atmosphere of argon must be used. To apply the PBF-LB/M method, the selected alloy must be in powder form, which for this case must be very fine, dense, uniform in size, chemically homogeneous, and as round as possible [48–50]. There are several metallurgical methods for obtaining metal powders. One of the more accessible and inexpensive methods is the mechanical alloying process (MA), which involves the milling of pure chemical element powders ( $\geq 99.00\%$  purity). Even if there are research works that use the gas-atomization method to obtain powder for additive manufacturing processes, the present work wanted to demonstrate the fact that by using mechanical alloying, it is also possible to obtain an appropriate quality of samples processed through PBF-LB/ m. Using the mechanical alloying method, the obtained powder can attempt a nanocrystalline or even amorphous structure because the milling process implies a multitude of severe plastic deformations and provokes the repeated fracturing and cold welding of the component particles [51–53].

For the present study, we proposed a biodegradable alloy, Mg-10Zn-0.8Ca-0.5Zr (%wt.), not tested before by other group of researchers, obtained in a powder state by mechanical alloying, and processed through PBF-LB/M. The aim of the work is to obtain adequate microstructural, mechanical and corrosion characteristics suitable for bone implants. The present study represents a complementary research work to anterior published [54,55] papers, which, at this time, are mainly based on mechanical and corrosion analysis, with a summary microstructural analysis. In addition to the objective stated above, possible

research limitations could appear for this incipient experimental program due to the new selected processing route with specific conditions—mechanical alloying followed by PBF-LB/M—applied to a new compositional type of a biodegradable Mg-based alloy.

## 2. Materials and Methods

### 2.1. Mechanical Alloying—First Applied Procedure for Obtaining the Alloy Powder

To obtain the magnesium alloy in powder form, the mechanical alloying method was applied. The chemical elements selected for alloying the magnesium alloy were zinc, zirconium and calcium. In order to carry out the mechanical alloying procedure, chemical elements were used in powder form, with a purity of 99.00%, and an average diameter of the powders as follows: Mg < 100  $\mu\text{m}$ , Zn < 40–50  $\mu\text{m}$ , Zr < 40–50  $\mu\text{m}$  and granules of Ca. The chemical composition calculated to be obtained was Mg-10Zn-0.8Ca-0.5Zr (%wt.). The amounts of alloying elements were chosen in such a way as to agree with those already reported in the specialized literature and discussed above in the Introduction.

The applied mechanical alloying procedure (schema in Figure 1—right) involves milling the above powder mixture in the established proportions, using a planetary mill (a PM 100 Retsch type, Haan, Germany) of high-energy, with a capacity of 500 mL and an applied frequency of 50–60 Hz.

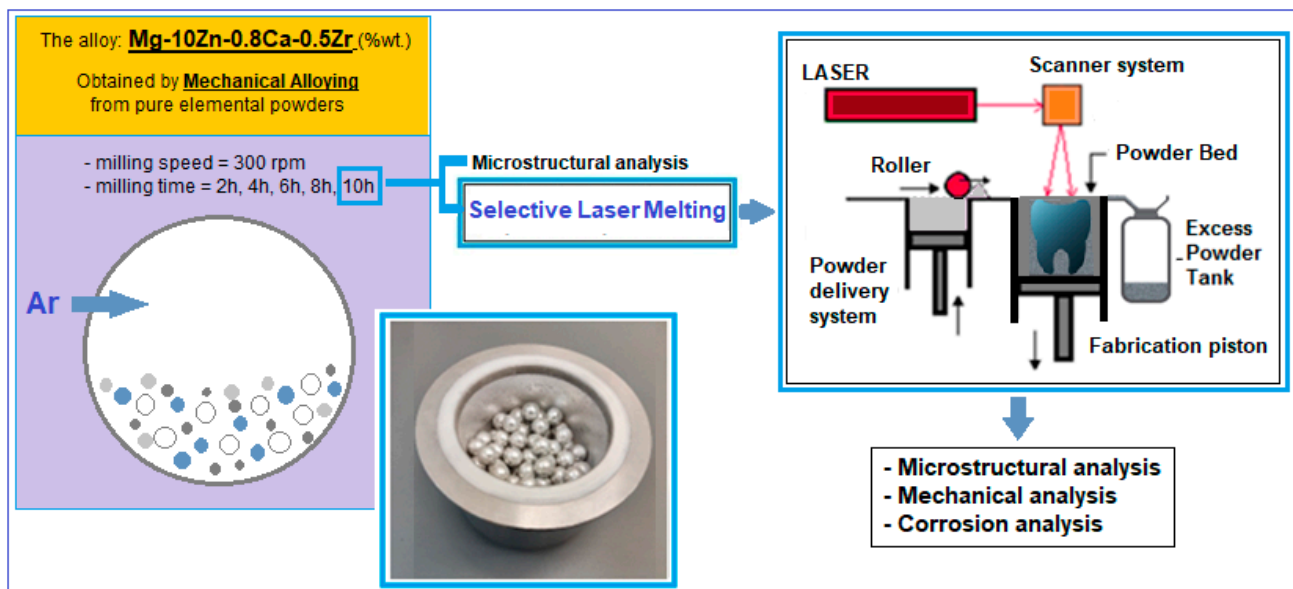


**Figure 1.** Schema of the experimental program performed for the alloy Mg-10Zn-0.8Ca-0.5Zr.

The milling speed is usually applied between 150 and 350 rpm; for the present case, a value of 300 rpm was applied. To enhance the milling effect, zirconium oxide balls with a diameter of approx. 10 mm, with a weight ratio of 10:1, were added to the powder mixture. For oxidation protection, the argon atmosphere of 1.5 bar overpressure was used. Also, during the milling process, the cold welding of the powder particles can occur; to prevent this phenomenon, 5% n-heptane solution was added. For the present experimental test, the variable parameter was the milling time. Increasing times from two-to-two hours were tested, starting from 2 h to 10 h. The objective was to finally obtain a powder alloy with a chemical composition and a microstructure as homogeneous and consistent as possible. Therefore, the milling time was extended as much as possible.

After the mechanical alloying procedure, the obtained powder alloy was subjected to a sieving operation with smaller and smaller dimensions; the final one was <30  $\mu\text{m}$ .

## 2.2. Selective Laser Melting (SLM)—Second Applied Procedure for Obtaining a Bulk Specimen from the Alloy Powder

The finest powder obtained after mechanical alloying was subjected to AM through the PBF-LB/M method (schema in Figure 1—left).

For that, the laser used was of the MYSINT 100-3D Selective Laser Fusion type (SISMA s.p.a., Vicenza, Italy), which is a laser special dedicated to printing metallic powder. The applied parameters were the following; laser power—40–150 W; laser speed—300–1000 mm/s; layer height—20–30  $\mu\text{m}$ ; volumetric energy density—100–550 J/mm<sup>3</sup>; and inert gas, nitrogen and argon were used. Several samples with dimensions of 10 × 10 × 12 mm (length × width × height) were obtained in order to be further tested in SEM analysis (one sample), compression tests (nine samples) and corrosion tests (three samples).

## 2.3. Microstructural and Mechanical Analysis of the Studied Mg-Alloy Processed by PBF-LB/M

The microstructural analysis of the Mg-Zn-Ca-Zr alloy (in its powder state and after PBF-LB/M processing) started with a SEM-SE (scanning electron microscopy—secondary electron)-imaging investigation that was performed using a Tescan VEGA II-XMU SEM microscope (Tescan Orsay Holding a.s. Brno, Czech Republic). Concomitant calculations of powder characteristics, such as dimension, morphology and homogeneity, were made. The XRD (X-ray diffraction) analysis was performed at room temperature (RIGAKU Mini-Flex600, Tokyo, Japan) using Cu-K $\alpha$  radiation with a scattering angle  $2\theta$  in the range of 30–90 degrees for a step size of 0.02 degrees. Nine samples of the studied Mg-Zn-Ca-Zr alloy, after the PBF-LB/M printing procedure, were subjected to the compression test by using a universal testing machine of the INSTRON 3382 type (Instron Ltd., High Wycombe, Buckinghamshire, HP123SY, Birmingham, UK). The samples were subjected to constantly increasing loads until they finally broke.

## 2.4. Corrosion Analysis of the Studied Mg-Alloy Processed by SLM

The corrosion monitoring was carried out using a potentiostat (Radiometer Analytical VoltaLab PGZ 402, Lyon, France). Three corrosion tests were conducted: open-circuit potential, electrochemical impedance spectroscopy (EIS), and polarisation for corrosion (Tafel plots) [56]. The open-circuit-potential tests were determined for the studied Mg alloy; EIS was measured using a value that was 200 mV more electropositive than that determined during open-circuit-potential tests (AC signal impedance acquisition was performed for EIS tests, using an AC sine wave amplitude of 2 mV), and the polarisation for the corrosion test was performed using a range from −1600 mV to +1600 mV and a scan rate of 2 mV/s; the potentiostat's software (VoltaMaster 4, version 7.9) provided the following data, using a preset calculation method (1st Stern method: Tafel): the corrosion rate ( $V_{\text{CORR}}$ ), the corrosion current ( $i_{\text{CORR}}$ ), the polarization resistance ( $R_p$ ), the electrode potential ( $E_{(i=0)}$ ) and the anodic and cathodic Tafel constants ( $\beta_a$  and  $\beta_c$ ). The tests were performed in triplicate.

## 3. Results and Discussions

### 3.1. Microstructural Characterization of the Mg-Zn-Ca-Zr Alloy in Powder State and after PBF-LB/M Processing

As already stated in the Introduction, in the previously published articles [54,55] the preponderance was the microstructural analysis of the studied alloy. In the article [54], the emphasis was placed on the step-by-step follow-up of the morphological and compositional evolution of the powder alloy obtained through mechanical alloying by varying the milling time. In the second article [55], the microstructural evolution of the subsequent AM samples using the PBF-LB/M method by varying the volumetric energy-density parameter was highlighted. The present work tries to take a step forward by deepening the research regarding the mechanical behaviour of the same alloy processed by PBF-LB/M as well as the corrosion resistance of this alloy. Thus, the microstructural analysis was performed, but this time, only on the samples that showed the best previous results: first, on the alloy powder obtained through mechanical alloying, with a milling time of 10 h; then, on

the samples obtained after PBF-LB/M processing, applying a volumetric energy density (VED) of  $134 \text{ J/mm}^3$  and a scanning speed of  $600 \text{ mm/s}$ , as two parameters with important influence.

Figure 2 shows two representative SEM images obtained after microscopic analysis of the studied Mg-Zn-Ca-Zr alloy in its powder state, as it has resulted from the mechanical alloying procedure with a milling time of 10 h. Looking at the powder morphology, several important features were observed using a SEM-calibrated microscope.

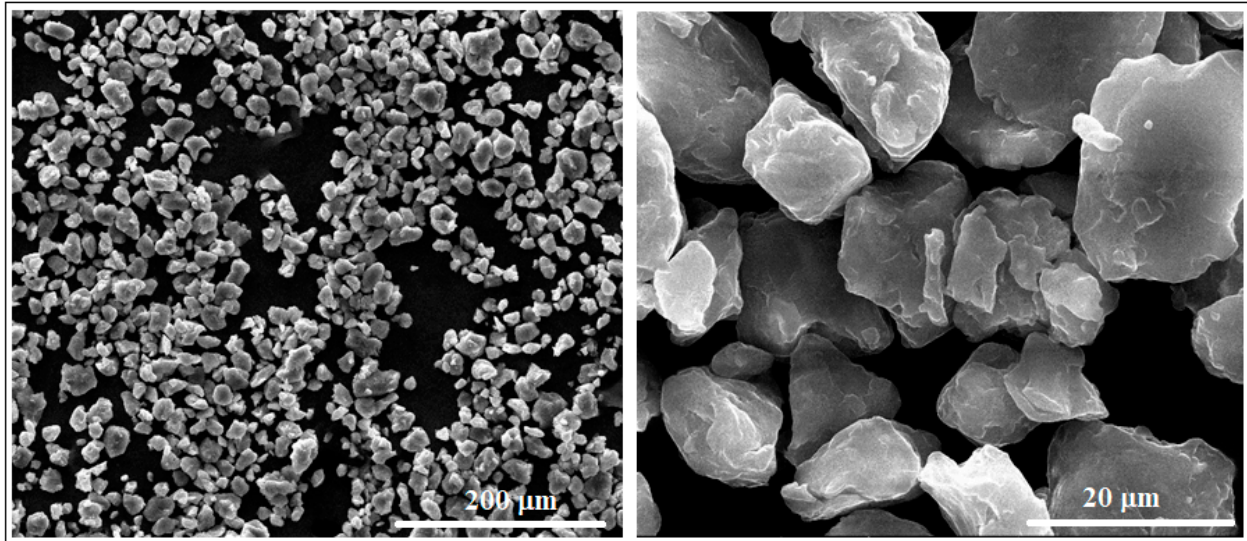


**Figure 2.** The SEM-SE images for the Mg-Zn-Ca-Zr powder alloy after mechanical alloying with a milling time of 10 h.

First, it is a dimensional homogeneity of the powder particles with an average value of  $16.2 \pm 8.6 \mu\text{m}$ . In conformity with [42–44], this average dimension is satisfactory for the subsequent PBF-LB/M procedure.

A second important characteristic refers to the surface of the powder particles that looks to be homogeneous, with a uniform colour and without signs of inhomogeneities; the structure consists of a single phase, with alloying elements completely solubilized in magnesium and, consequently, without secondary phases. Moreover, the lack of secondary phases and the complete solubilization of the alloying elements was also proven by XRD analysis (Figure 3), which indicates patterns corresponding to the magnesium-based solid solution,  $\alpha\text{-Mg}$ . Keeping in mind that for the present case, the amount of zinc exceeds the limit of solubility in Mg (6.2%wt.), if the synthesis procedure had followed the classic line of alloy obtaining (melting–solidification) then the secondary phase  $\text{MgZn}_2$  should have been formed. Unlike the classic version, during the mechanical alloying procedure, there are severe plastic deformations of the powder particles, accompanied by cold welding and their strong and constant fractures, which give rise to a strong energy that can lead to a homogeneous distribution of the chemical elements in the Mg-powder particles. There are works, such as [57], which clearly confirm this possibility, and even for the extreme case where the amorphous structure can be obtained [58] at much longer milling times, about 70 h or more. In the present case, the total absence of  $\text{MgZn}_2$  in the XRD patterns cannot be absolutely guaranteed for the real structure, considering the possible minute amount of precipitate formed, and the low sensitivity of the device used.

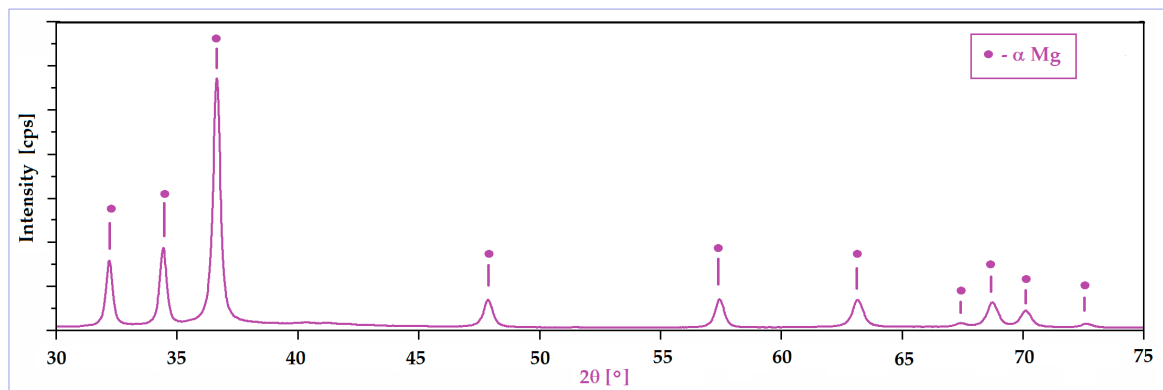


**Figure 3.** The XRD spectra of the Mg-Zn-Ca-Zr powder alloy after mechanical alloying with a milling time of 10 h.

Finally, another positive morphological characteristic observed was that, unlike the shorter milling times for which sharper shapes of the alloy powders are observed, at 10 h, no agglutinated particles were observed, having an individualized appearance, with regular, smooth and relatively rounded shapes. Therefore, all these particular characteristics can be considered to have been suitable for the subsequent PBF-LB/M process for which, in general, a fine powder with a homogeneous and almost rounded shapes is required.

Figure 4 shows some representative SEM images obtained by the microscopic analysis of the Mg-Zn-Ca-Zr alloy after the PBF-LB/M procedure. The initial macroscopic examination of the obtained PBF-LB/M samples of  $10 \times 10 \times 12$  mm shows a robust state, but is relatively porous and without cracks that correspond to the proposed objective—to obtain a structure that can reproduce that of cortical bone.

In that sense, the examination by SEM analysis was made inside of the PBF-LB/M samples, in order to observe the homogeneous distribution of the robustness and porosity, cumulatively, in the entire volume of the samples. From the SEM images corresponding to Figure 4, it can be seen that the examined surfaces, exposed to a gradually increasing magnification, show a dense and unbreakable morphology, without the balling effect, known to be detrimental to the mechanical performance and therefore undesirable.

The degree of porosity obtained by the PBF-LB/M procedure must be correlated with a real and therefore desired level of cortical bone porosity. This “desired” level can be set/standardized depending on the type and location of the bone implant and can be achieved by a judicious selection of PBF-LB/M processing parameters. However, for the present case, the PBF-LB/M samples, judging by their morphological condition, can be considered suitable for an early examination of their mechanical and corrosion performance.

### 3.2. Mechanical Characterization of the Mg-Zn-Ca-Zr Alloy in Its Powder State and after PBF-LB/M Processing

Compression tests were applied for a set of nine samples realized by PBF-LB/M processing. Figure 5 shows the macroscopic dimensional aspect of some samples, before and after testing. The strain–stress curves for each of all nine tested samples are presented all together in Figure 6. After processing the data resulting from these curves, the determination of the mechanical characteristics was made for all tested samples. Thus, Figure 7 shows the representative strain–stress curve resulting from weighting the data from all tested samples, and Table 1 shows the average corresponding values for the maximum compressive strength ( $\sigma_{\max}$ ), deformation to fracture ( $\epsilon_{\max}$ ) and elastic modulus (E). The standard deviation was calculated and has been included in Table 1.

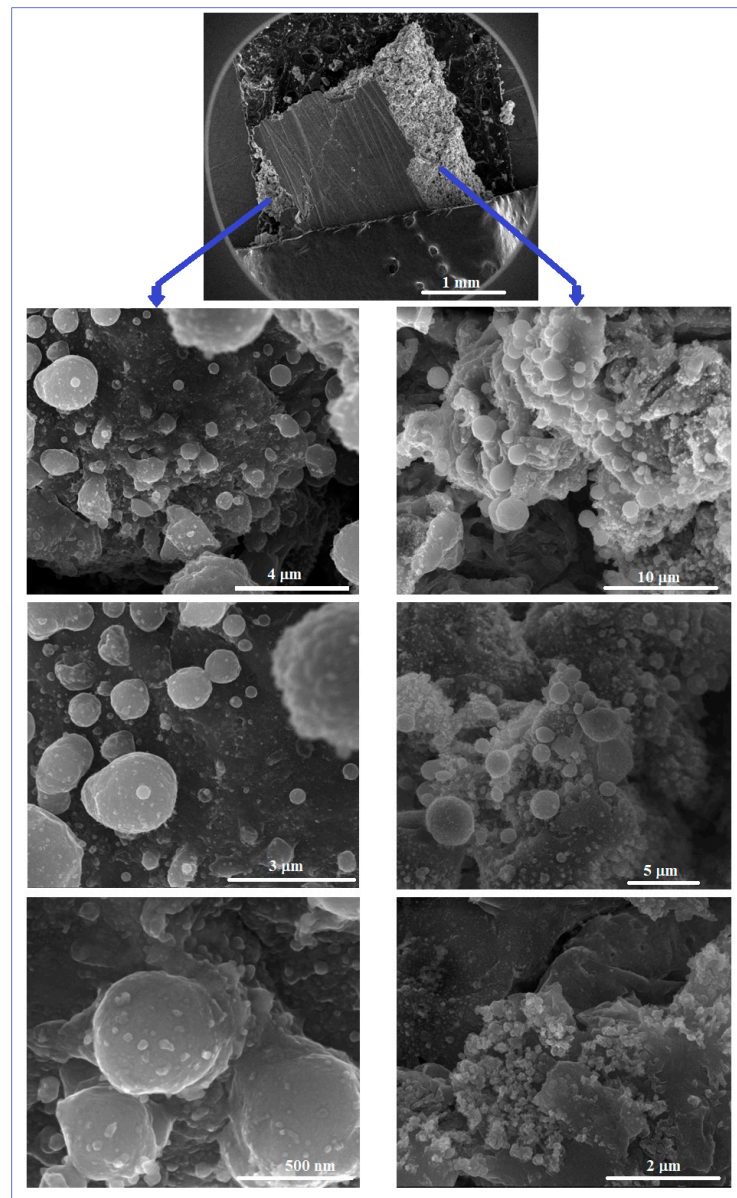


**Figure 4.** The SEM-SE images for the Mg-Zn-Ca-Zr alloy after PBF-LB/M processing.

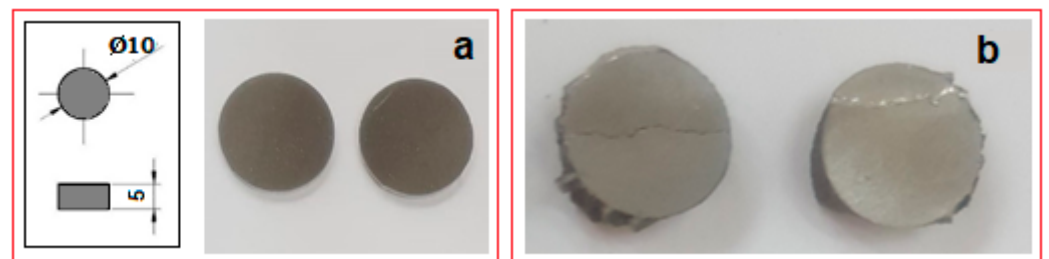


**Figure 5.** Macroscopic views of the PBF-LB/M samples (a) before and (b) after compression tests.

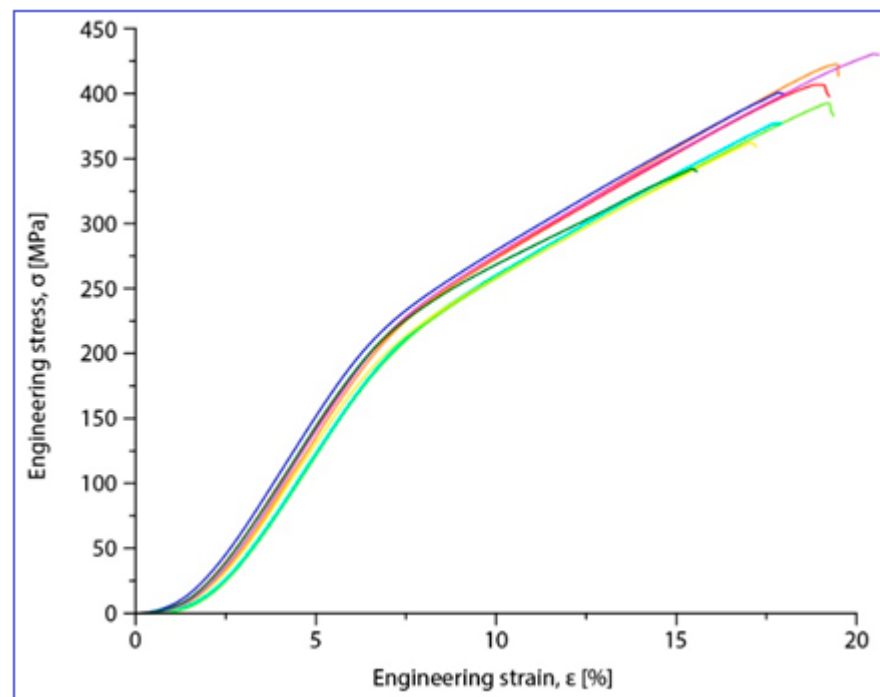


Figure 6. Stress–strain diagrams for the nine PBF-LB/M samples tested in compression tests.

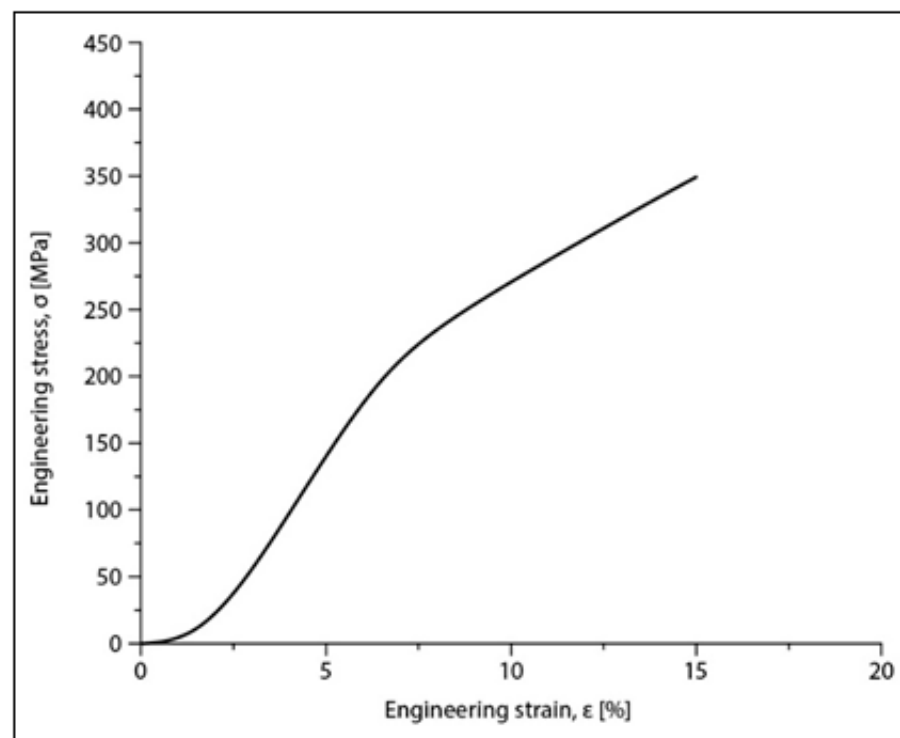


Figure 7. Stress–strain diagram for the Mg-Zn-Ca-Zr alloy in the PBF-LB/M condition after compression tests.

Table 1. Mechanical properties of the studied alloy after PBF-LB/M processing: ultimate compressive strength ( $\sigma_{\max}$ ); deformation to fracture ( $\epsilon_{\max}$ ); elastic modulus (E); SD (Standard Deviation).

The Alloy in PBF-LB/M Condition	$\sigma_{\max}$ [MPa]	$\epsilon_{\max}$ [%]	E [GPa]
Mg-10Zn-0.8Ca-0.5Zr (%wt.)	$381.25 \pm 17.19$	$17.92 \pm 0.44$	$42.10 \pm 1.08$

Examining the data in Table 1, it can be said that the values obtained for the main mechanical properties are generally close to those of cortical bone [8,9], especially for the Young's modulus (30 GPa for cortical bone compared to 42 GPa for the tested samples). This means that, for an implant made of this alloy, using PBF-LB/M technology that ensures a certain desired porosity of the material, the risk of the stress-shielding phenomenon is very low, especially if the implant is designed to be biodegradable over time.

### 3.3. Corrosion Analysis of the PBF-LB/M-Processed Mg-Based Alloy

For the corrosion test, three samples of studied Mg alloy after AM using the PBF-LB/M procedure were used. These three samples were tested in PBS (Phosphate-buffered saline) solution with three different pH values (based on Roth Roti<sup>®</sup>CELL PBS CELLPURE<sup>®</sup>, having the composition 154.004 mM NaCl, 5.599 mM Na<sub>2</sub>HPO<sub>4</sub>, 1.058 mM KH<sub>2</sub>PO<sub>4</sub>), with the intention of covering the widest possible range of pH variation in the human body: (1) stock PBS [59] solution with a pH of 7.4; (2) HCl (0.1M)-doped PBS with a pH of 3.16 and (3) KOH (pellets)-doped PBS with a pH of 10.1. All tests were conducted using Ag/AgCl (3M KCl) as a reference electrode, a Pt wire electrode as counter electrode, and the samples as the working electrode. For each pH, three different immersion times were tested: 0 h, 24 h and 48 h. During all performed tests, an important amount of hydrogen emission was observed—Figure 8. After the corrosion tests were concluded, each of three electrochemical cells were stored in a digital drying oven at 37 °C.

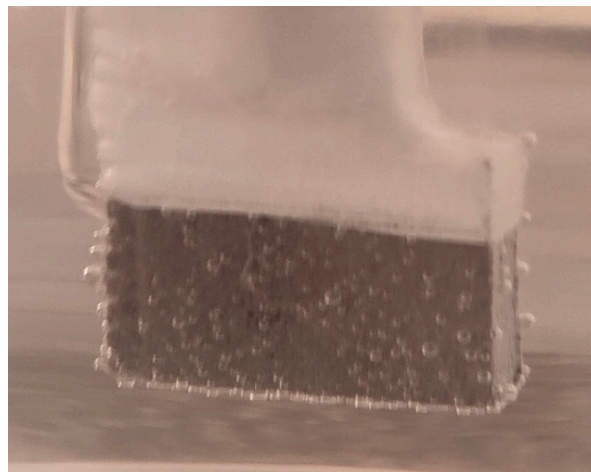


**Figure 8.** Hydrogen bubbles released on the surface of the working electrode (sample).

Figures 9–11 show the Nyquist, Bode and Tafel spectra obtained for the tested samples. The resulting Nyquist spectra have a convulsing/trembling shape due to the noise generated by the massive amounts of hydrogen release. These hydrogen bubbles adhered to the surface of the sample and, as such, interfered with the readings during the tests performed, as seen in Figure 8. The generation of hydrogen, inevitable in the case of magnesium alloys, can create a considerable variability in the results, unfortunately; this situation can be augmented, in addition, by the high level of roughness of the surface of the PBF-LB/M samples, a sine qua non condition, by which the generation of hydrogen is higher than in the case of the more compact surfaces of the samples. This roughness is assumed in this case, out of the desire to imitate the more porous surface of the cortical bone that will support the joining with a biodegradable implant made of such a magnesium alloy. Being an accelerated corrosion test, finally, all samples were dissolved and formed a dark grey precipitate on the bottom of their respective electrochemical cells.

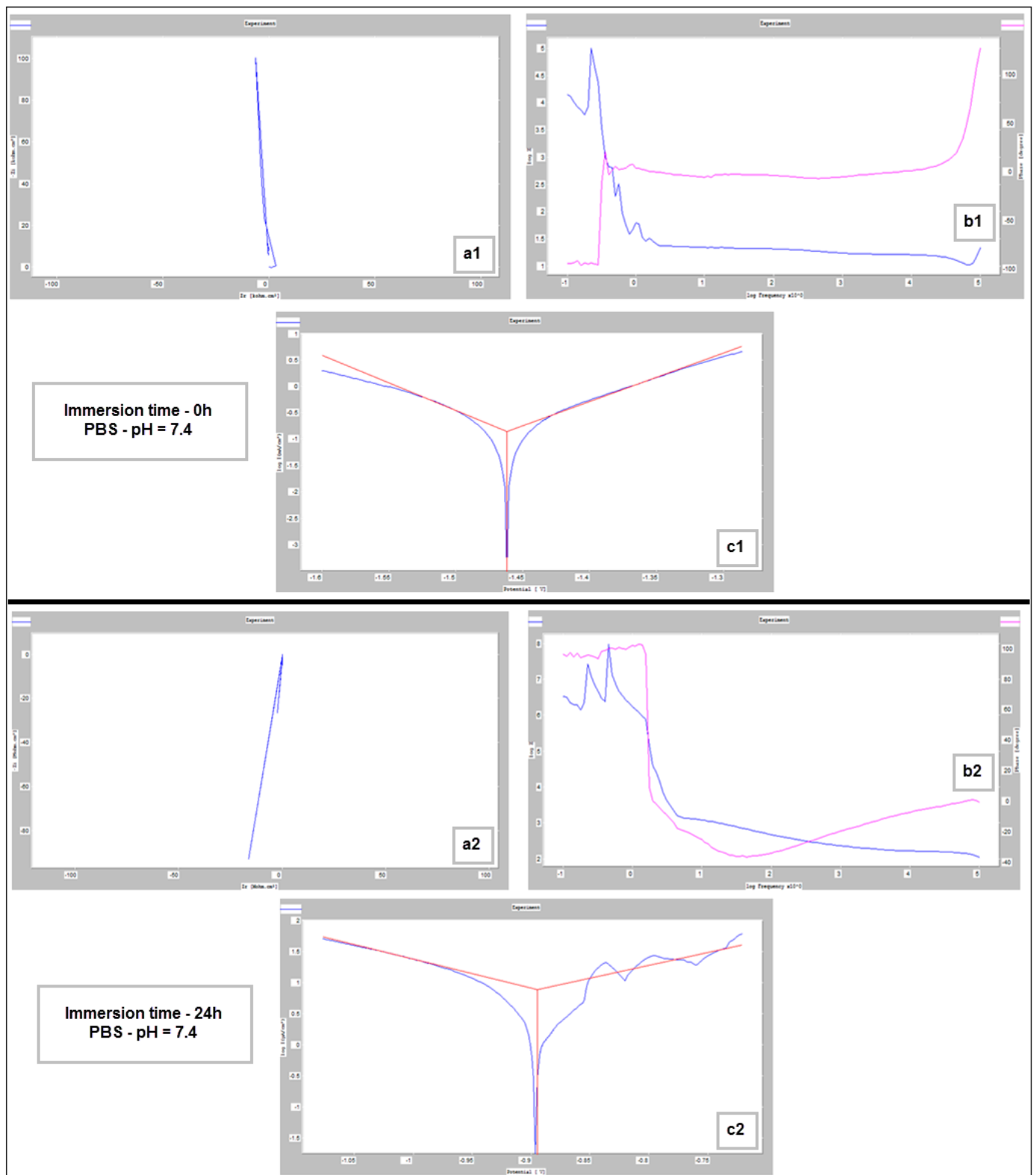


**Figure 9.** Nyquist (a1,a2), Bode (b1,b2) and Tafel (c1,c2) diagrams for the PBF-LB/M sample tested in PBS with pH 7.4, at immersion times of 0 h and 24 h.

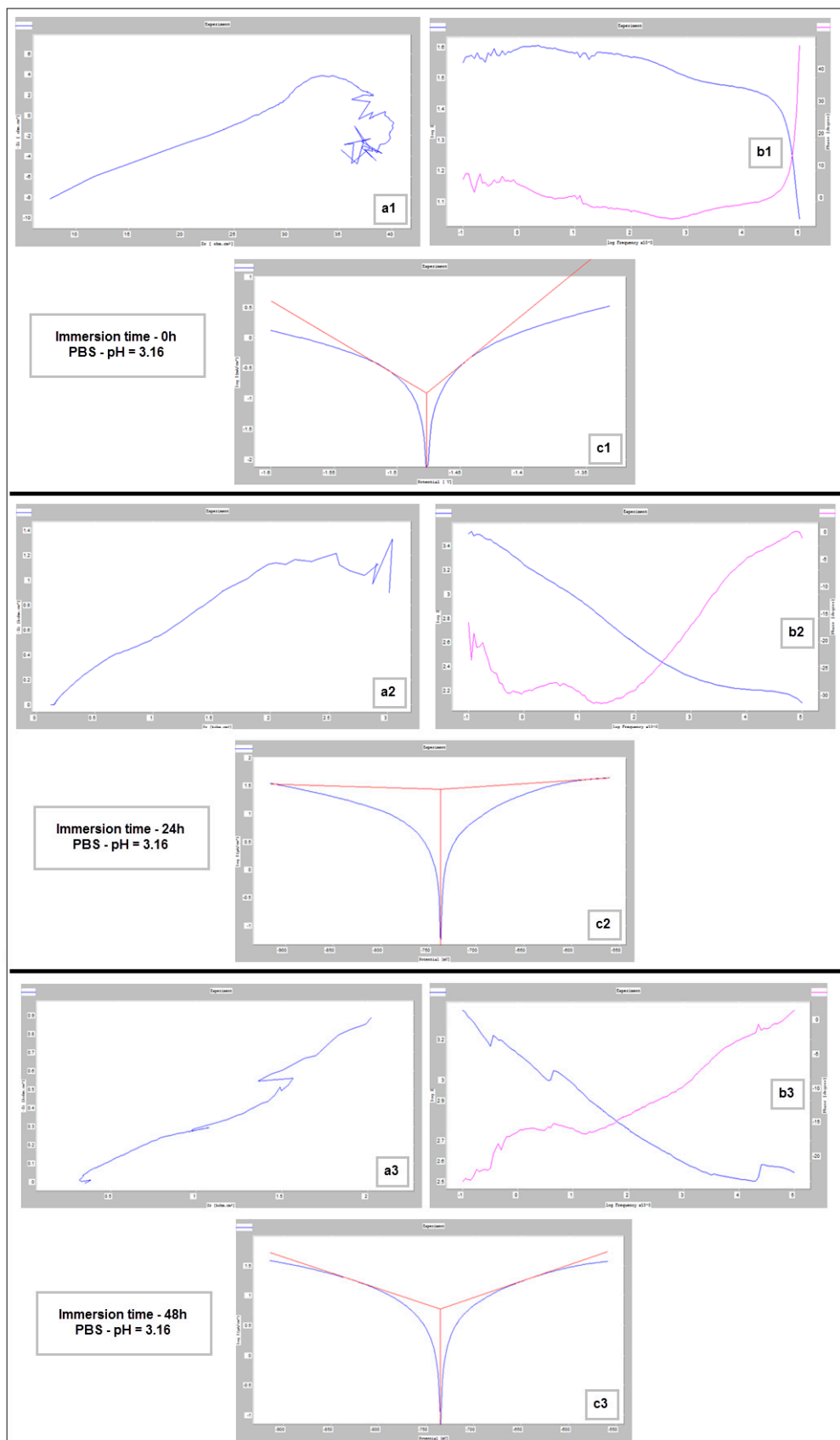


**Figure 10.** Nyquist (a1–a3), Bode (b1–b3) and Tafel (c1–c3) diagrams for PBF-LB/M sample tested in PBS with pH 3.16, at immersion times of 0 h, 24 h and 48 h.

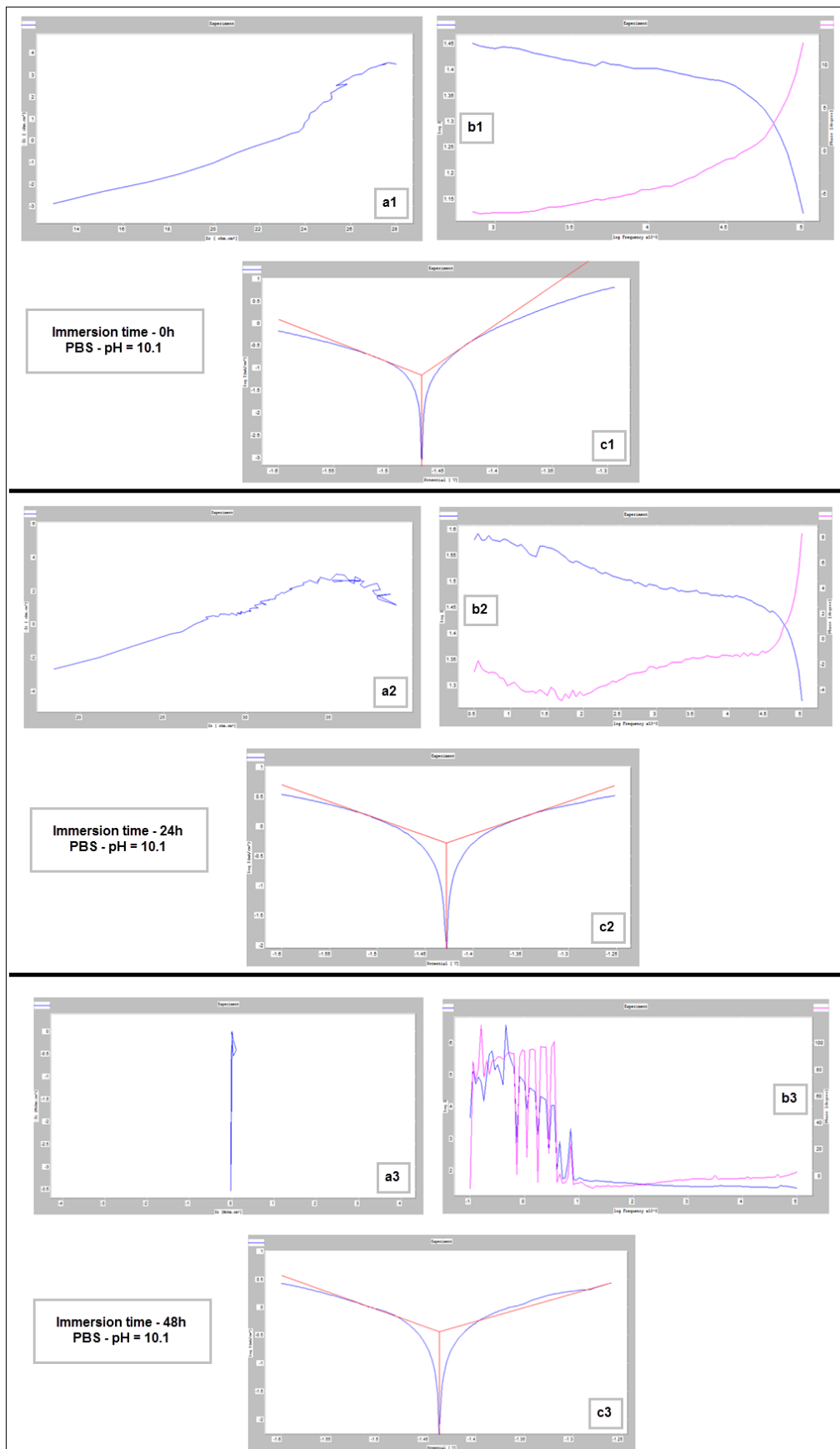


**Figure 11.** Nyquist (a1–a3), Bode (b1–b3) and Tafel (c1–c3) diagrams for PBF-LB/M sample tested in PBS with pH 10.1, at immersion times of 0 h, 24 h and 48 h.

The main parameters determined, which resulted from these corrosion analyses, are shown in Table 2: the corrosion current ( $j_{\text{corr}}$ ), the electrode potential ( $E_{(i=0)}$ ) and the corrosion rate ( $V_{\text{corr}}$ ). The resulting corrosion-rate values for each tested sample are indicated in Figure 12.

**Table 2.** Main corrosion parameters for tested PBF-LB/M samples in PBS solution, with three different pH values and different immersion times.

Mg-Alloy, PBF-LB/M-Processed, Immersed in PBS with pH:	Immersion Time (h)	$V_{\text{corr}}$ (mm/Year)	$I_{\text{corr}}$ (mA/cm <sup>2</sup> )	Potential $E_{(i=0)}$ (mV)
pH = 7.4	0	1.426 ± 0.04	0.139 ± 0.026	-1462.1 ± 2.1
	24	0.079 ± 0.01	0.007 ± 0.001	-895 ± 1.3
	48	-	-	-
pH = 3.16	0	1.252 ± 0.04	0.122 ± 0.016	-1476.4 ± 2.1
	24	0.278 ± 0.02	0.027 ± 0.004	-737.9 ± 1.1
	48	0.060 ± 0.01	0.005 ± 0.001	-735 ± 1.1
pH = 10.1	0	0.703 ± 0.06	0.068 ± 0.002	-1469.6 ± 2.8
	24	5.305 ± 0.12	0.517 ± 0.022	-1428 ± 2.2
	48	3.679 ± 0.10	0.359 ± 0.013	-1437.6 ± 2.4

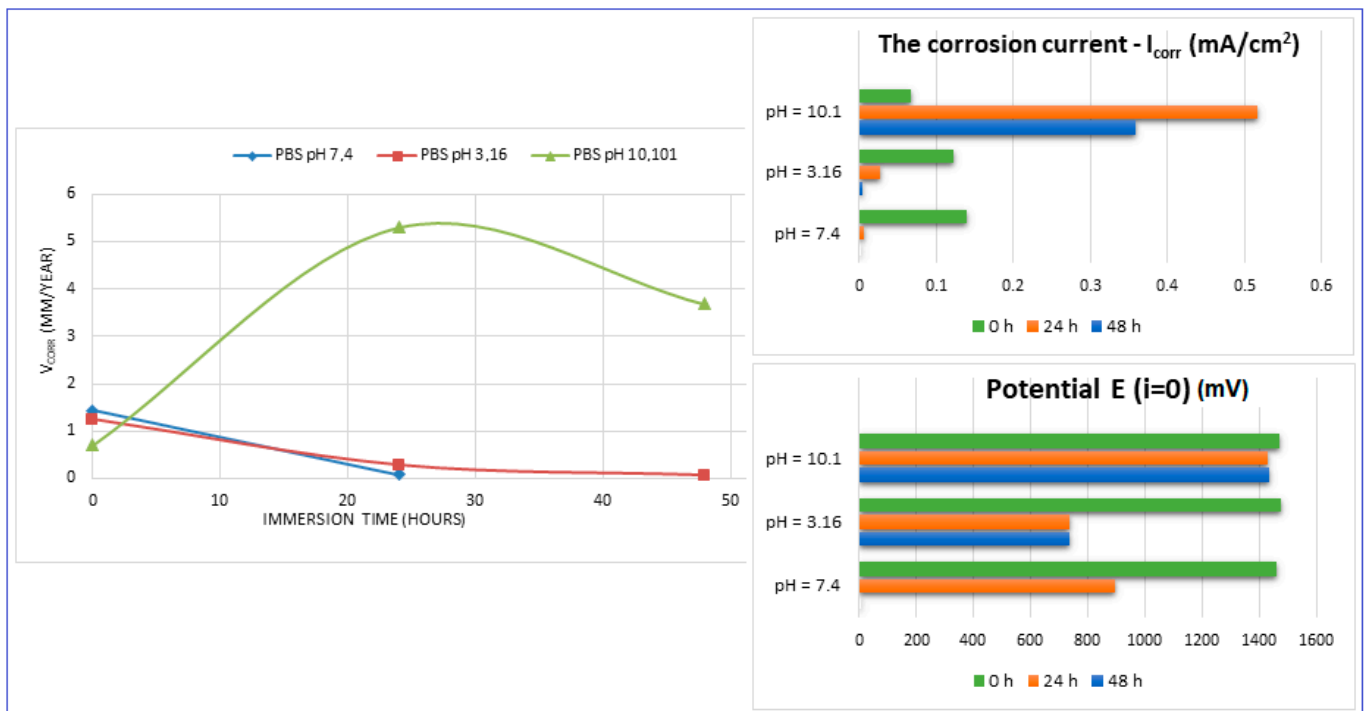


**Figure 12.** The evolution of the corrosion rate for the tested samples.

For increasing the corrosion performance of a metallic alloy, it was generally established that the electrode potential must have an upward trend (it should be high), and the corrosion current must be low [60–62]. This fact can be seen from the values of Table 2. A similarity in the corrosion parameters’ evolution can be seen for both neutral and acidic pH. If we compare these values with those corresponding to the commercial ZK60 alloy (around 1.45 mm/year [63–68]), it can be found that the values obtained here can be considered quite satisfactory.

For basic pH (10.1), however, notable differences are observed: the electrode potential and the current density have a fluctuating variation (increase/decrease), and the resulting

corrosion rates are outside the ranges generally reported. This fact is highlighted by Figure 12 also. These types of inadvertences can probably be attributed to the fact that the hydrogen release was not measured. It should be pointed out that the PBS solution with a basic pH (10.1) represents an experimental situation and not a real physiologic test, as done for real regular implants. However, the alkalization can occur in the case of Mg-based implants reaching a pH level of ten and even higher [69,70]. Moreover, in conformity to [7], it seems that the corrosion rate can be substantially improved by expanding the solubility of the alloying elements using non-equilibrium techniques, without causing the serious micro-galvanic corrosion that usually is generated when the added alloying elements' precipitates as second-phase particles. The mechanical alloying procedure, used for the present experimental program, can be considered a non-equilibrium technique, because the amount of zinc exceeds the limit of solubility in Mg (10%wt. instead of 6.2%wt.) through severe plastic deformations that occur during the process.

However, as a good result noted from these experiments, it should be mentioned and emphasized that at a neutral pH, the corrosion rate of the Mg-10Zn-0.8Ca-0.5Zr alloy (1.426 mm/year) is very close to that of the alloy considered an etalon for comparison with nowadays —ZK 60 (1.45 mm/year) [63–68].

#### 4. Conclusions

A magnesium alloy with the composition of Mg-10Zn-0.8Ca-0.5Zr (%wt.) has been obtained via mechanical alloying using pure elemental powders. After 10 h of milling in an argon atmosphere, the obtained powder alloy reveals a uniform dimensional homogeneity with an average particle size of  $16.2 \pm 8.6 \mu\text{m}$  and no agglutinated particles. The powder particles have also a homogeneous microstructure, with a uniform colour and no agglutinated particles. This powder alloy has been processed by additive manufacturing using the PBF-LB/M method.

The SEM microstructural analysis of the PBF-LB/M samples reveal a dense and unbreakable morphology, but with a porosity able to reproduce that of cortical bone, and without the undesirable balling effect.

After compression tests, the alloy samples in the PBF-LB/M condition have a Young's modulus of 42 GPa, close to that of cortical bone, 30 GPa, avoiding the stress-shielding effect.

The PBF-LB/M samples tested for corrosion resistance in PBS solution with three different pH values show that the corrosion parameters have a satisfactory evolution. At the normal neutral-body pH, the corrosion rate of the Mg-10Zn-0.8Ca-0.5Zr alloy (1.426 mm/year) is very close to that of the ZK 60 alloy (1.45 mm/year).

**Author Contributions:** Conceptualization, D.R., A.N. and V.D.C.; methodology, R.E.H.; software, V.A.R. and S.I.D.; validation, D.R., A.N. and V.D.C.; formal analysis, D.R.; investigation, D.S., S.I., N.S., V.A.R., E.M.C. and R.S.C.; resources, V.D.C.; data curation, S.I.D.; writing—original draft preparation, A.N. and D.S.; writing—review and editing, A.N. and D.R.; visualization, D.R., V.D.C., A.N., S.I.D., R.E.H., D.S., S.I., V.A.R., N.S., E.M.C. and R.S.C.; supervision, D.R. and A.N.; project administration, D.R. and V.D.C.; funding acquisition, D.R. and V.D.C. All authors have read and agreed to the published version of the manuscript.

**Funding:** This research was funded by Romanian National Authority for Scientific Research, CCCDI—UEFISCDI, Project ERANET-MANUNET-AMMBI/grant no. 207/2020.

**Institutional Review Board Statement:** Not applicable.

**Informed Consent Statement:** Not applicable.

**Data Availability Statement:** The data presented in this study are available on request from the corresponding author.

**Acknowledgments:** The authors acknowledge financial support for this research by the Romanian National Authority for Scientific Research CCCDI—UEFISCDI, Project ERANET-MANUNET-AMMBI/grant no. 207/2020.

**Conflicts of Interest:** The authors declare no conflicts of interest.

## References

1. Esmaily, M.; Svensson, J.E.; Fajardo, S.; Birbilis, N.; Frankel, G.S.; Virtanen, S.; Arrabal, R.; Thomas, S.; Johansson, L.G. Fundamentals and advances in magnesium alloy corrosion. *Prog. Mater. Sci.* **2017**, *89*, 92–193. [[CrossRef](#)]
2. Song, J.; She, J.; Chen, D.; Pan, F. Latest research advances on magnesium and magnesium alloys worldwide. *J. Magnes. Alloy.* **2020**, *8*, 1–41. [[CrossRef](#)]
3. Lovašiová, P.; Lovaši, T.; Kubásek, J.; Jablonská, E.; Msallamová, Š.; Michalcová, A.; Vojtěch, D.; Suchý, J.; Koutný, D.; Alzubi, E.G.H. Biodegradable WE43 Magnesium Alloy Produced by Selective Laser Melting: Mechanical Properties, Corrosion Behavior, and In-Vitro Cytotoxicity. *Metals* **2022**, *12*, 469. [[CrossRef](#)]
4. Chen, X.; Ning, S.; Wang, A.; Le, Q.; Liao, Q.; Jia, Y.; Cheng, C.; Li, X.; Atrens, A.; Yu, F. Microstructure, mechanical properties and corrosion behavior of quasicrystal-reinforced Mg-Zn-Y alloy subjected to dual-frequency ultrasonic field. *Corros. Sci.* **2020**, *163*, 108289. [[CrossRef](#)]
5. Zhang, J.; Zhang, B.; Zhang, J.; Lin, W.; Zhang, S. Magnesium Promotes the Regeneration of the Peripheral Nerve. *Front. Cell Dev. Biol.* **2021**, *9*, 717854. [[CrossRef](#)] [[PubMed](#)]
6. Dong, J.; Lin, T.; Shao, H.; Wang, H.; Wang, X.; Song, K.; Li, Q. Advances in degradation behavior of biomedical magnesium alloys: A review. *J. Alloys Compd.* **2022**, *908*, 164600. [[CrossRef](#)]
7. Cao, F.; Xiao, B.; Wang, Z.; Ying, T.; Zheng, D.; Atrens, A.; Song, G.-L. A Mg alloy with no hydrogen evolution during dissolution. *J. Magnes. Alloy.* **2023**, *11*, 2084–2095. [[CrossRef](#)]
8. Li, W.; Qiao, W.; Liu, X.; Bian, D.; Shen, D.; Zheng, Y.; Wu, J.; Kwan, K.Y.H.; Wong, T.M.; Cheung, K.M.C.; et al. Biomimicking Bone-Implant Interface Facilitates the Bioadaptation of a New Degradable Magnesium Alloy to the Bone Tissue Microenvironment. *Adv. Sci.* **2021**, *8*, 2102035. [[CrossRef](#)] [[PubMed](#)]
9. Amukarimi, S.; Mozafari, M. Biodegradable magnesium-based biomaterials: An overview of challenges and opportunities. *MedComm* **2021**, *2*, 123–144. [[CrossRef](#)] [[PubMed](#)]
10. Banerjee, P.C.; Al-Saadi, S.; Choudhary, L.; Harandi, S.E.; Singh, R. Magnesium Implants: Prospects and Challenges. *Materials* **2019**, *12*, 136. [[CrossRef](#)] [[PubMed](#)]
11. O'Neill, E.; Awale, G.; Daneshmandi, L.; Umerah, O.; Lo, K.W.-H. The roles of ions on bone regeneration. *Drug Discov. Today* **2018**, *23*, 879–890. [[CrossRef](#)] [[PubMed](#)]
12. Qin, Y.; Wen, P.; Guo, H.; Xia, D.; Zheng, Y.; Jauer, L.; Poprawe, R.; Voshage, M.; Schleifenbaum, J.H. Additive manufacturing of biodegradable metals: Current research status and future perspectives. *Acta Biomater.* **2019**, *98*, 3–22. [[CrossRef](#)] [[PubMed](#)]
13. Zhou, H.; Liang, B.; Jiang, H.; Deng, Z.; Yu, K. Magnesium-based biomaterials as emerging agents for bone repair and regeneration: From mechanism to application. *J. Magnes. Alloy.* **2021**, *9*, 779–804. [[CrossRef](#)]
14. Zhang, T.; Wang, W.; Liu, J.; Wang, L.; Tang, Y.; Wang, K. A review on magnesium alloys for biomedical applications. *Front. Bioeng. Biotechnol.* **2022**, *10*, 953344. [[CrossRef](#)] [[PubMed](#)]
15. Wang, J.L.; Xu, J.K.; Hopkins, C.; Chow, D.H.K.; Qin, L. Biodegradable Magnesium-Based Implants in Orthopedics—A General Review and Perspectives. *Adv. Sci.* **2020**, *7*, 1902443. [[CrossRef](#)] [[PubMed](#)]
16. Wang, W.; Han, P.; Peng, P.; Zhang, T.; Liu, Q.; Yuan, S.-N.; Huang, L.-Y.; Yu, H.-L.; Qiao, K.; Wang, K.-S. Friction Stir Processing of Magnesium Alloys: A Review. *Acta Met. Sin. (Engl. Lett.)* **2020**, *33*, 43–57. [[CrossRef](#)]
17. Jung, O.; Porchetta, D.; Schroeder, M.-L.; Klein, M.; Wegner, N.; Walther, F.; Feyerabend, F.; Barbeck, M.; Kopp, A. In Vivo Simulation of Magnesium Degradability Using a New Fluid Dynamic Bench Testing Approach. *Int. J. Mol. Sci.* **2019**, *20*, 4859. [[CrossRef](#)] [[PubMed](#)]
18. Kumar, K.; Gill, R.S.; Batra, U. Challenges and opportunities for biodegradable magnesium alloy implants. *Mater. Technol.* **2018**, *33*, 153–172. [[CrossRef](#)]
19. Chin, P.Y.Y.; Cheok, Q.; Glowacz, A.; Caesarendra, W. A Review of In-Vivo and In-Vitro Real-Time Corrosion Monitoring Systems of Biodegradable Metal Implants. *Appl. Sci.* **2020**, *10*, 3141. [[CrossRef](#)]
20. Kim, Y.-K.; Lee, K.-B.; Kim, S.-Y.; Bode, K.; Jang, Y.-S.; Kwon, T.-Y.; Jeon, M.H.; Lee, M.-H. Gas formation and biological effects of biodegradable magnesium in a preclinical and clinical observation. *Sci. Technol. Adv. Mater.* **2018**, *19*, 324–335. [[CrossRef](#)] [[PubMed](#)]
21. Kuhlmann, J.; Bartsch, I.; Willbold, E.; Schuchardt, S.; Holz, O.; Hort, N.; Höche, D.; Heineman, W.R.; Witte, F. Fast escape of hydrogen from gas cavities around corroding magnesium implants. *Acta Biomater.* **2013**, *9*, 8714–8721. [[CrossRef](#)] [[PubMed](#)]
22. Huan, Z.G.; Leeflang, M.A.; Zhou, J.; Fratila-Apachitei, L.E.; Duszczuk, J. In vitro degradation behavior and cytocompatibility of Mg-Zn-Zr alloys. *J. Mater. Sci. Mater. Med.* **2010**, *21*, 2623–2635. [[CrossRef](#)] [[PubMed](#)]
23. Gu, X.; Xie, X.; Li, N.; Zheng, Y. In vitro and in vivo studies on a Mg-Sr binary alloy system developed as a new kind of bio-degradable metal. *Acta Biomater.* **2012**, *8*, 2360–2374. [[CrossRef](#)] [[PubMed](#)]
24. Seifen, S.; Hock, M. Development of magnesium implants by application of conjoint-based quality function deployment. *J. Biomed. Mater. Res.* **2019**, *107*, 2814–2834. [[CrossRef](#)] [[PubMed](#)]
25. Shuai, C.; Zhou, Y.; Yang, Y.; Gao, C.; Peng, S.; Wang, G. Ag-Introduced Antibacterial Ability and Corrosion Resistance for Bio-Mg Alloys. *BioMed Res. Int.* **2018**, *2018*, 6023460. [[CrossRef](#)] [[PubMed](#)]

26. Seetharaman, S.; Sankaranarayanan, D.; Gupta, M. Magnesium-Based Temporary Implants: Potential, Current Status, Applications, and Challenges. *J. Funct. Biomater.* **2023**, *14*, 324. [CrossRef]
27. Li, X.; Liu, X.; Wu, S.; Yeung, K.; Zheng, Y.; Chu, P.K. Design of magnesium alloys with controllable degradation for biomedical implants: From bulk to surface. *Acta Biomater.* **2016**, *45*, 2–30. [CrossRef] [PubMed]
28. Sezer, N.; Evis, Z.; Kayhan, S.M.; Tahmasebifar, A.; Koça, M. Review of magnesium-based biomaterials and their applications. *J. Magnes. Alloy.* **2018**, *6*, 23–43. [CrossRef]
29. Global Personalized 3D Printed Orthopedic Implants Market, Data Bridge Market Research. Available online: <https://www.databridgemarketresearch.com/reports/global-personalized-3d-printed-orthopedic-implants-market> (accessed on 8 December 2023).
30. Roohani, N.; Hurrell, R.; Kelishadi, R.; Schulin, R. Zinc and its importance for human health: An integrative review. *J. Res. Med. Sci.* **2013**, *18*, 144–157. Available online: <https://www.researchgate.net/publication/27120142> (accessed on 16 December 2023).
31. Zhang, M.; Chen, C.; Liu, C.; Wang, S. Study on Porous Mg-Zn-Zr ZK61 Alloys Produced by Laser Additive Manufacturing. *Metals* **2018**, *8*, 635. [CrossRef]
32. Liu, C.; Zhang, M.; Chen, C. Effect of laser processing parameters on porosity, microstructure and mechanical properties of porous Mg-Ca alloys produced by laser additive manufacturing. *Mater. Sci. Eng. A* **2017**, *703*, 359–371. [CrossRef]
33. Bitá, T.; Corneschi, I.; Ungureanu, E.; Bitá, A.I.; Ignat, N.D.; Dura, H.; Carstoc, I.D.; Nicolcescu, P. Influence of heat treatment on microstructure and corrosion behavior of biodegradable Mg-Ca alloy. *U.P.B. Sci. Bull. Ser. B* **2023**, *85*. Available online: [https://www.scientificbulletin.upb.ro/rev\\_docs\\_arhiva/full9d8\\_327223.pdf](https://www.scientificbulletin.upb.ro/rev_docs_arhiva/full9d8_327223.pdf) (accessed on 22 November 2023).
34. Ikeo, N.; Nishioka, M.; Mukai, T. Fabrication of biodegradable materials with high strength by grain refinement of Mg–0.3 at.% Ca alloys. *Mater. Lett.* **2018**, *223*, 65–68. [CrossRef]
35. Deng, M.; Wang, L.; Snihirova, D.; Bohlen, J.; Kurz, G.; Lamaka, S.V.; Höche, D.; Zheludkevich, M.L. Micro-alloyed Mg-Ca: Corrosion susceptibility to heating history and a plain problem-solving approach. *J. Magnes. Alloy.* **2023**, *11*, 1193–1205. [CrossRef]
36. Wang, J.; Dou, J.; Wang, Z.; Hu, C.; Yu, H.; Chen, C. Research progress of biodegradable magnesium-based biomedical materials: A review. *J. Alloys Compd.* **2022**, *923*, 166377. [CrossRef]
37. Allameh, S.H.; Emamy, M. The Effect of Ca Content on the Microstructure, Hardness and Tensile Properties of AZ81 Mg Cast Alloy. *J. Mater. Eng. Perform.* **2017**, *26*, 2151–2161. [CrossRef]
38. Shi, L.; Chen, S.; Zheng, F.; Liu, M.; Yang, H.; Zhang, B. Corrosion resistance evaluation of biodegradable magnesium alloy vascular stents optimized by mechanical adapted polymer coating strategy. *Colloids Surfaces A Physicochem. Eng. Asp.* **2023**, *658*, 130664. [CrossRef]
39. Nowosielski, R.; Gawlas-Mucha, A.; Borowski, A.; Guwer, A. Fabrication and properties of magnesium based alloys Mg-Ca. *JAMME* **2013**, *61*, 367–374.
40. Shuai, C.; Yang, Y.; Wu, P.; Lin, X.; Liu, Y.; Zhou, Y.; Feng, P.; Liu, X.; Peng, S. Laser rapid solidification improves corrosion behavior of Mg-Zn-Zr alloy. *J. Alloys Compd.* **2017**, *691*, 961–969. [CrossRef]
41. Nayeb-Hashemi, A.A.; Clark, J.B. The Mg–Zr (Magnesium-Zirconium) system. *Bull. Alloy. Phase Diagr.* **1985**, *6*, 246–250. [CrossRef]
42. Manic, M.; Vitković, N.; Mitic, J. Design and manufacturing of the personalized plate implants. In *Personalized Orthopedics*; Canciglieri Junior, O., Trajanovic, M.D., Eds.; Springer: Cham, Switzerland, 2022. [CrossRef]
43. Jariwala, S.H.; Lewis, G.S.; Bushman, Z.J.; Adair, J.H.; Donahue, H.J. 3D Printing of Personalized Artificial Bone Scaffolds. *3D Print. Addit. Manuf.* **2015**, *2*, 56–64. [CrossRef] [PubMed]
44. Nopová, K.; Jaroš, J.; Červinek, O.; Pantělejev, L.; Gneiger, S.; Senck, S.; Koutný, D. Processing of AZ91D Magnesium Alloy by Laser Powder Bed Fusion. *Appl. Sci.* **2023**, *13*, 1377. [CrossRef]
45. Yang, Y.; Ping, W.; Xin, L.; Yong, L.; Hong, B.; Zhou, Y.; Gao, C.; Shuai, C. System development, formability quality and microstructure evolution of selective laser-melted magnesium. *Virtual Phys. Prototyp.* **2016**, *11*, 173–181. [CrossRef]
46. Chen, L.; Lin, Z.; Wang, M.; Huang, W.; Ke, J.; Zhao, D.; Yin, Q.; Zhang, Y. Treatment of trauma-induced femoral head necrosis with biodegradable pure Mg screw-fixed pedicle iliac bone flap. *J. Orthop. Transl.* **2019**, *17*, 133–137. [CrossRef] [PubMed]
47. Karunakaran, R.; Ortgies, S.; Tamayol, A.; Bobaru, F.; Sealy, M.P. Additive manufacturing of magnesium alloys. *Bioact. Mater.* **2020**, *5*, 44–54. [CrossRef] [PubMed]
48. Hassan, S.F.; Islam, M.T.; Saheb, N.; Baig, M.M.A. Magnesium for Implants: A Review on the Effect of Alloying Elements on Biocompatibility and Properties. *Materials* **2022**, *15*, 5669. [CrossRef] [PubMed]
49. Chen, J.; Xu, Y.; Kolawole, S.K.; Wang, J.; Su, X.; Tan, L.; Yang, K. Systems, Properties, Surface Modification and Applications of Biodegradable Magnesium-Based Alloys: A Review. *Materials* **2022**, *15*, 5031. [CrossRef] [PubMed]
50. Zhao, D.; Witte, F.; Lu, F.; Wang, J.; Li, J.; Qin, L. Current status on clinical applications of magnesium-based orthopaedic implants: A review from clinical translational perspective. *Biomaterials* **2017**, *112*, 287–302. [CrossRef]
51. Lesz, S.; Hrapkowicz, B.; Karolus, M.; Gołombek, K. Characteristics of the Mg-Zn-Ca-Gd Alloy after Mechanical Alloying. *Materials* **2021**, *14*, 226. [CrossRef] [PubMed]
52. Salleh, E.M.; Ramakrishnan, S.; Hussain, Z. Synthesis of Biodegradable Mg-Zn Alloy by Mechanical Alloying: Effect of Milling Time. *Procedia Chem.* **2016**, *19*, 525–530. [CrossRef]
53. Abbasi, M.; Sajjadi, S.A.; Azadbeh, M. An investigation on the variations occurring during Ni3Al powder formation by mechanical alloying technique. *J. Alloys Compd.* **2010**, *497*, 171–175. [CrossRef]

54. Raducanu, D.; Cojocaru, V.D.; Nocivin, A.; Hendea, R.E.; Ivanescu, S.; Stanciu, D.; Trisca-Rusu, C.; Serban, N.; Drob, S.I.; Campian, R.S. Microstructure Evolution during Mechanical Alloying of a Biodegradable Magnesium Alloy. *Crystals* **2022**, *12*, 1641. [[CrossRef](#)]
55. Hendea, R.E.; Raducanu, D.; Nocivin, A.; Ivanescu, S.; Stanciu, D.; Trisca-Rusu, C.; Campian, R.S.; Drob, S.I.; Cojocaru, V.D.; Gălbinașu, B.M. Laser Powder Bed Fusion Applied to a New Biodegradable Mg-Zn-Zr-Ca Alloy. *Materials* **2022**, *15*, 2561. [[CrossRef](#)] [[PubMed](#)]
56. Park, K.; Chang, B.-Y.; Hwang, S. Correlation between Tafel Analysis and Electrochemical Impedance Spectroscopy by Prediction of Amperometric Response from EIS. *ACS Omega* **2019**, *4*, 19307–19313. [[CrossRef](#)] [[PubMed](#)]
57. Suryanarayana, C. Mechanical Alloying: A Novel Technique to Synthesize Advanced Materials. *Research* **2019**, *2019*, 4219812. [[CrossRef](#)] [[PubMed](#)]
58. Lesz, S.; Kremzer, M.; Gołombek, K.; Nowosielski, R. Influence of milling time on amorphization of mg-zn-ca powders synthesized by mechanical alloying technique. *Arch. Metall. Mater.* **2018**, *63*, 845–851. [[CrossRef](#)]
59. Lichtenauer, M.; Nickl, S.; Hoetzenecker, K.; Mangold, A.; Moser, B.; Zimmermann, M.; Hacker, S.; Niederpold, T.; Mitterbauer, A.; Ankersmit, H.J. Phosphate Buffered Saline Containing Calcium and Magnesium Elicits Increased Secretion of Interleukin-1 Receptor Antagonist. *Lab. Med.* **2009**, *40*, 290–293. [[CrossRef](#)]
60. Ouyang, Y.; Chen, Z.; Jiang, C.; Yang, W.; Chen, Y.; Yin, X.; Liu, Y. Design of the double-layer biocompatible coating on AZ31 magnesium alloy for highly effective corrosion resistance. *Surf. Coat. Technol.* **2021**, *428*, 127897. [[CrossRef](#)]
61. Ma, E. Alloys created between immiscible metals. *Prog. Mater. Sci.* **2005**, *50*, 413–509. [[CrossRef](#)]
62. Suryanarayana, C.; Liu, J. Processing and characterization of mechanically alloyed immiscible metals. *Int. J. Mater. Res.* **2012**, *103*, 1125–1129. [[CrossRef](#)]
63. Fu, W.; Yang, H.; Li, T.; Sun, J.; Guo, S.; Fang, D.; Qin, W.; Ding, X.; Gao, Y.; Sun, J. Enhancing corrosion resistance of ZK60 magnesium alloys via Ca microalloying: The impact of nanoscale precipitates. *J. Magnes. Alloy.* **2023**, *11*, 3214–3230. [[CrossRef](#)]
64. Biancardi, O.V.; Luccas Rosa, V.; de Abreu, L.B.; Tavares, A.P.R.; Corrêa, R.G.; Cavalcanti, P.H.; Napoleão, B.I.; da Silva, E.P. Corrosion behavior of as-cast ZK60 alloy modified with rare earth addition in sodium sulfate medium. *Corros. Sci.* **2019**, *158*, 108092.
65. Mandal, M.; Mondal, K. Effect of Micro-alloying and Microstructure on the Corrosion Behavior of As-Cast Mg-6.2 wt.% Zn Alloy. *J. Mater. Eng. Perform.* **2020**, *29*, 6691–6700. [[CrossRef](#)]
66. Xue, Y.; Pang, X.; Karparvarfard, S.M.H.; Jahed, H.; Luo, S.; Shen, Y. Corrosion Protection of ZK60 Wrought Magnesium Alloys by Micro-Arc Oxidation. *Metals* **2022**, *12*, 449. [[CrossRef](#)]
67. Merson, D.; Vasiliev, E.; Markushev, M.; Vinogradov, A. On the corrosion of ZK60 magnesium alloy after severe plastic deformation. *Lett. Mater.* **2017**, *7*, 421–427. [[CrossRef](#)]
68. Merson, E.; Poluyanov, V.; Myagkikh, P.; Merson, D.; Vinogradov, A. Fractographic features of technically pure magnesium, AZ31 and ZK60 alloys subjected to stress corrosion cracking. *Mater. Sci. Eng. A* **2020**, *772*, 138744. [[CrossRef](#)]
69. Hassan, H.W.; Rahmati, M.; Barrantes, A.; Haugen, H.J.; Mirtaheri, P. In Vitro Monitoring of Magnesium-Based Implants Degradation by Surface Analysis and Optical Spectroscopy. *Int. J. Mol. Sci.* **2022**, *23*, 6099. [[CrossRef](#)] [[PubMed](#)]
70. Qin, J.; Shi, X.; Li, H.; Zhao, R.; Li, G.; Zhang, S.; Ding, L.; Cui, X.; Zhao, Y.; Zhang, R. Performance and failure process of green recycling solutions for preparing high degradation resistance coating on biomedical magnesium alloys. *Green Chem.* **2022**, *24*, 8113–8130. [[CrossRef](#)]

**Disclaimer/Publisher’s Note:** The statements, opinions and data contained in all publications are solely those of the individual author(s) and contributor(s) and not of MDPI and/or the editor(s). MDPI and/or the editor(s) disclaim responsibility for any injury to people or property resulting from any ideas, methods, instructions or products referred to in the content.